Advances in Radiation Oncology (2025) **10**, 101757

advances in radiation oncology

www.advancesradonc.org

Scientific Article

Deep Learning-Based Heterogeneity Correction of the Homogeneous Dose Distribution for Single Brain Tumors in Gamma Knife Radiosurgery

Sangyoon Lee, BA, Shubhendu Mishra, MD, and Yoichi Watanabe, PhD*

Department of Radiation Oncology, University of Minnesota Medical School, Minneapolis, Minnesota

Received 19 August 2024; accepted 3 March 2025

Purpose: Heterogeneity correction is vital in radiation therapy treatment planning to ensure accurate dose delivery. Brain cancer stereotactic treatments, like Gamma Knife radiosurgery (GKRS), often rely on homogeneous water-based calculations despite the potential heterogeneity impact near bony structures. This study aims to develop a method for generating synthetic dose plans incorporating heterogeneity effects without additional computed tomography (CT) scans.

Methods and Materials: Magnetic resonance imaging and CT images, TMR10-based, and convolution-based dose distributions were used from 100 retrospectively collected and 22 prospectively collected GKRS patients. A conditional Generative Adversarial Network was trained to translate TMR10 into synthetic convolution (sConv) doses.

Results: The generated sConv dose demonstrated qualitative and quantitative similarity to the actual convolution (Conv) dose, showcasing better agreement of dose distributions and improved isodose volume similarity with the Conv dose in comparison to the TMR10 dose (γ pass rate; sConv dose, 92.43%; TMR10 dose, 74.18%. Prescription isodose dice; sConv dose, 91.7%; TMR10 dose, 89.7%). Skull-induced scatter and attenuation effects were accurately reflected in the sConv dose, indicating the usefulness of the new dose prediction model as an alternative to the time-consuming convolution dose calculations.

Conclusions: Our deep learning approach offers a feasible solution for heterogeneity-corrected dose planning in GKRS, circumventing additional CT scans and lengthy calculation times. This method's effectiveness in preserving dose distribution characteristics in a heterogeneous medium while only requiring a homogeneous dose plan highlights its utility for including the process in the routine treatment planning workflows. Further refinement and validation with diverse patient cohorts can enhance its applicability and impact in clinical settings.

Introduction

Heterogeneity correction is essential in radiation therapy treatment planning to accurately estimate the dose delivery.[1-3] Beams penetrating a heterogeneous medium other than water, such as lungs and bones, exhibit perturbed dose distributions depending on the location and thickness of the heterogeneous medium.[1-3] Various approaches have been explored and implemented to consider the heterogeneity of different tissues for treatment planning. Whereas heterogeneous treatment planning for lungs has been well developed, as the lung is vulnerable to

This manuscript is based on work previously presented at the 66th Annual Meeting of the American Association of Physicists in Medicine (AAPM), held in Los Angeles, California in 2024, as a poster titled "Prediction of Heterogeneous Treatment Planning in Gamma Knife Radiosurgery Using Homogeneous Plan with Conditional Generative Adversarial Network."

Sources of support: This work had no specific funding.

This work is originated at the Department of Radiation Oncology, University of Minnesota Medical School, MN, USA. Data generated or analyzed during the study are available from the corresponding author by request with permission of the Institutional Review Board.

*Corresponding author: Yoichi Watanabe, PhD; Email: watan016@umn.edu

https://doi.org/10.1016/j.adro.2025.101757

significant heterogeneity effect, stereotactic treatment of brain tumors, including Gamma Knife radiosurgery (GKRS), is less highlighted for heterogeneity effect.[1,2,4] The brain is known to be not much affected by the heterogeneity effect, and homogeneous water medium-based calculations with magnetic resonance imaging (MRI) using the TMR10 algorithm (TMR10 dose) are currently accepted as the standard in GKRS planning.[1,2,4]

Nevertheless, there are cases when the heterogeneity, especially near the bony skulls, significantly impacts the dose distribution.[4] Heterogeneity-corrected treatment plans cannot be made from the MRI data because it does not contain electron density information. The convolution (Conv) dose calculation method available in the GKRS treatment planning system, Leksell GammaPlan, can be used to consider the heterogeneity effects adequately with additional CT scans. However, the CT scans cause added radiation dose to healthy brain regions and extra time for scanning. Moreover, the calculation time of the convolution algorithm rapidly increases as the tumor volume increases, which could take up to several minutes for the Conv dose compared to < 1 minute calculation time for the TMR10 dose.[2,3] Therefore, generating synthetic doses, including the heterogeneity effects (synthetic convolution [sConv] dose) without CT scans, is desired for rapid treatment planning in routine clinical settings.

Recently, deep learning image generation has been intensively investigated, improving deep learning performance in medical imaging applications.[5,6] Several studies have employed deep learning with convolutional neural networks (CNNs) to generate synthetic dose plans.[7-13] Generative models have also demonstrated groundbreaking abilities in image generation, including image-to-image translation and augmentation, showing great potential in the medical imaging domain.[5,7-13] Generative adversarial networks (GANs) and, more recently, diffusion models have shown comparable or more effective generation of images than CNNs, leveraging the adversarial training algorithm and diffusion process to learn the high-dimensional distribution of complex data.[6,14,15] Recent studies implementing diffusion models outperformed GANs and CNNs in generating realistic doses.[7,8] However, developing clinically acceptable deep learning tools remains challenging because of imperfect structure matching, affecting the dose distribution.[7-12] Some studies generated synthetic CT from MRI to calculate the dose in heterogeneous media in treatment planning systems.[16,17] Although synthetic CT can produce a realistic dose, the lengthy dose calculation time still impedes the inclusion of the more accurate dose calculation algorithm in the routine clinical setting. Furthermore, several studies have used resized dose distributions of 128×128 instead of the complete 512×512,[7,8] which hinders the precise and accurate evaluation of the dose distribution and their isodose lines.

To solve the problem, we used the GAN-based image-to-image translation method. Our generator gets a 512×512-sized TMR10 dose as an input to generate a synthetic convolution (sConv) dose. The conditional discriminator performs adversarial training to make the generator produce an authentic sConv dose. The image-to-image translation method employs the benefit of TMR10 dose as the input, and the model learns the accurate dose distribution. We made qualitative and quantitative comparisons of the sConv dose to the Conv dose to show effective translation from the TMR10 dose to the sConv dose. Isodose lines of different dose images were presented, and gamma index (γ) pass rates were reported to demonstrate clinical usefulness. Additionally, the effects of the skull-to-tumor distances and tumor sizes on the dose prediction were evaluated.

Methods and Materials

This study (IRB: 0810M293942) was approved by our institution's Institutional Review Board, and written informed consent was obtained from all patients to disclose their information for our study.

Data collection and processing

MR images, CT images, and TMR10-based and convolution-based dose distributions were retrospectively collected from 148 patients with various types of brain tumors who received GKRS from 2019 to 2022. The same data sets of 29 patients treated from 2023 to 2024 were prospectively collected. The GammaPlan version for dose calculations with TMR10 and Convolution algorithms was 11.1.1 or newer. MR and CT images were coregistered for every patient, and then transformation matrices from the CT images to MRI were used to map the Conv dose to the same space as the TMR10 dose. After visual inspection excluded misregistered data, 100 and 22 patients out of the initial data sets of 148 and 29 were available for the subsequent training and validation, respectively. The axial slices of the retrospectively collected patients (n = 18,336 slices, 100 patients) were randomly divided into 5 cross-validation sets. The 5 partitions were made for each patient data set. The prospectively collected patients' data were assigned as an internal validation set (n = 3984 slices 22 patients). TMR10 and Conv dose data with originally $1 \times 1 \times 1$ mm voxel size were resampled to $512 \times 512 \times z$, where z is the slice thickness of scanning. Normalization by the maximum TMR10 dose from the entire data set was performed with all dose data, resulting in the dose from 0 to 1.

Deep learning model for dose distribution prediction

The conditional GAN was implemented based on Pix2Pix[18] with a ResNet generator and a Patch-GAN discriminator (Fig. 1A). The generator had the TMR10 dose

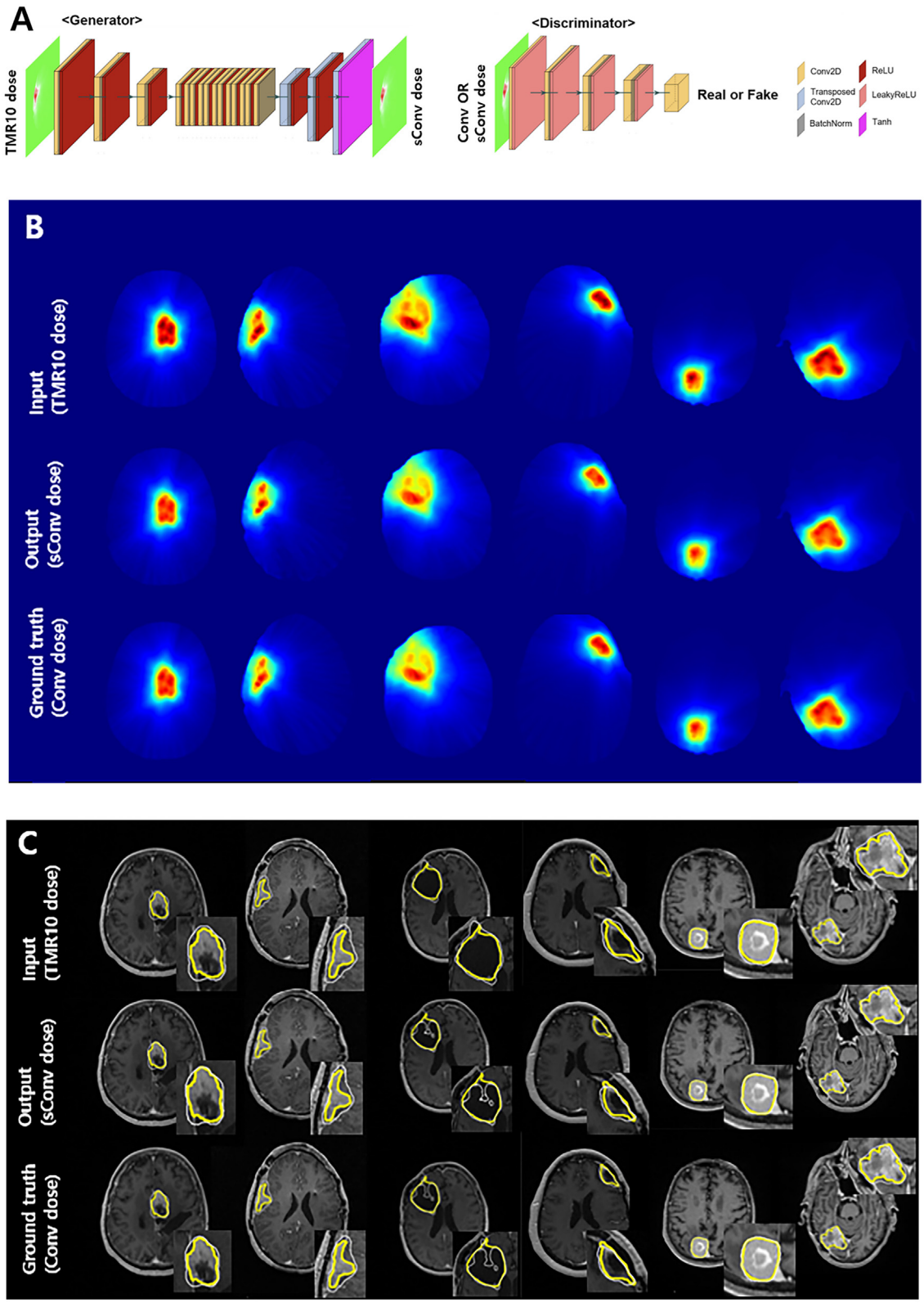

Figure 1 Model architecture and visualization of model outputs. (A) Conditional GAN model pipeline of generator and discriminator. (B) Qualitative results of image-to-image translation of TMR10 dose to sConv dose of different patients from test and internal validation sets. (C) Prescription isodose lines and tumor contour overlaid on MRI images (yellow = tumor, white = prescription isodose line). The cropped, magnified region of the interest is overlaid for each case.

Abbreviations: BatchNorm = Batch Normalization; Conv2D = Convolution 2D, MRI = magnetic resonance imaging; ReLU = Rectified Linear Unit; Tanh = Tanh activation; TransposedConv2D = Transposed Convolution 2D.

as its only input. It generated the sConv dose. TMR10 dose was then used as a conditional input to the conditional discriminator. Generator loss using L_1 and L_2 loss functions was calculated as an average loss for the discriminator's Conv dose and sConv dose classification. Discriminator loss was measured using a binary cross entropy loss. The default setting of Pix2Pix was used for training, and weights from epoch 60 were arbitrarily chosen for model validation. Training and inference were done with NVIDIA A100 at the Minnesota Supercomputer Institute. The inference took < 1 minute to compute the sConv doses for all slices of a patient.

Statistical analysis

The Dice similarity coefficient (DSC) was used to evaluate the isodose volume similarity between the TMR10, Conv, and sConv doses. The dose coverage of the tumor was assessed using 7 dosimetric metrics: the maximum tumor dose (D_{max}), the dose that 2 % or less of the tumor volume received (D_2), the dose that 50% of the tumor volume received (D_{50}), the mean tumor dose (D_{mean}), the dose that 98% of the tumor volume received (D_{98}), the minimum tumor dose (D_{min}), and the homogeneity index (HI).[7,8] To compare the dose distributions of Conv and sConv with the TMR10 dose distributions, we evaluated the γ pass rate[19] with a 1 mm/1% criterion for 3-dimensional dose data of every patient.

To assess the effect of the bone on the dose distributions, we specifically studied the dose to tumors whose skull-to-tumor distance was < 2 cm. Those tumors were named "tumors near the skull." Here, the "skull-to-tumor distance" was defined as the distance from the edge of the tumor to the closest point at the skull.[7] The DSC between the volumes covered by an isodose surface (named as isodose dice)[12] was also calculated for the comparison. The isodose dice, specifically for the prescription isodose level, was called "prescription isodose dice." The algorithm's performance was studied separately for small-sized tumors < 1 cm^3.[20] A Wilcoxon signed-rank test was used for statistical hypothesis testing. The null hypothesis was that there was no difference in 7 dosimetric metrics, the γ pass rates, and DSCs between the TMR10, Conv, and sConv doses. Additionally, the Bonferroni correction was applied for multiple comparisons.[21]

Results

Data characteristics of patients

Table 1 shows the overall demographic characteristics of the patients. A total of 100 patients' TMR10 and Conv dose data retrospectively collected were divided into 5 folds per patient (n = 18,336 slices; mean age, 62 years ± 13; 35 male) for cross-validation. An additional 22 patients prospectively collected were assigned as an internal validation set (n = 3984 slices; mean age, 67 years ±

Table 1 Data characteristics

Characteristic	Cross-validation set (n = 18,336; 100 Patients)	Internal validation set (n = 3984; 22 Patients)
Age, y	62 ± 13	67 ± 11
Sex		
Male	35 (35%)	15 (68%)
Female	65 (65%)	7 (32%)
Tumor size (cm^3)	13.79 ± 13.27	2.28 ± 1.22
Skull-to-tumor distance (cm)	3.07 ± 1.45	2.83 ± 1.13
Cancer types		
Met (solitary)	32	11
Mets (multiple)	33	6
Pituitary adenoma	1	0
Meningioma	17	4
Glomus tumor	2	0
Malignant glial tumor	5	1
Vestibular schwannoma	5	0
Other malignant tumor	2	0
Other benign tumor	1	0

11; 15 male). Various brain cancer types, such as metastatic tumors (solitary or multiple lesions), meningiomas, malignant glial tumors, and vestibular schwannomas, were included across the cross-validation and internal validation sets. Skull-to-tumor distances were 3.07 ± 1.45 cm and 2.83 ± 1.13 cm for cross-validation and internal validation sets, respectively. Average tumor volumes were 13.79 ± 13.27 cm^3 for the cross-validation set and 2.28 ± 1.22 cm^3 for the internal validation set.

Qualitative evaluation of the similarity between sConv and Conv doses

Examples of TMR10, Conv, and sConv doses from the cross-validation and internal validation sets are shown in Fig. 1B. Overall, the dose distributions of the sConv dose were visually more similar to the Conv dose than the TMR10 dose. In particular, hot spots in the TMR10 dose were not seen in the Conv or the sConv doses. In Fig. 1C, the prescription isodose lines (white) of TMR10, Conv, and sConv doses and the tumor contours (yellow) were overlaid on the MRI image. The isodose lines of the sConv dose were similar to those of the Conv dose, whereas there were more considerable differences between the isodose lines of the TMR10 and Conv doses. The second and third columns of Fig. 1C show a fully covered tumor area with the prescription dose for the TMR10 dose but not for the Conv or sConv doses. A subtle difference along the edge of the skull bone between the isodose lines of TMR10 and Conv dose was also seen in the sConv dose in the fourth column of Fig. 1C. Figure 2 shows magnified views of 7 isodose lines for the patient presented in the second column of Fig. 1C. Note that the 20-Gy isodose line (yellow) pointed by a white arrow indicates the area where the Conv and sConv doses were noticeably different from TMR10 dose, implying the significant heterogeneity effect on the dose because of a skull structure.

The dose-volume histogram (DVH) of the patient in Fig. 2 is shown in Fig. E1. The DVH line of the sConv dose was similar to the Conv dose, whereas the line of the TMR10 dose presented a different DVH profile. The difference map between the TMR10, Conv, and sConv doses in Fig. E2 showed the higher similarity of the sConv dose to the Conv dose than the TMR10 dose to the Conv dose. The improved similarity of the sConv dose to the Conv dose was well visualized in the tumor and near the skull locations in the difference maps.

Quantitative evaluation of the similarity between sConv and Conv doses

Evaluations of quantitative similarity between sConv and Conv doses (sConv vs Conv) and between TMR10 and Conv doses (TMR10 vs Conv) are shown in Table 2 for both the cross-validation and internal validation sets. With the internal validation set, the percentage difference (Δ%) of all dosimetric metrics between sConv and Conv doses was smaller than between TMR10 and Conv doses. The differences in Δ% between the 2 dose pairs (sConv vs Conv and TMR10 vs Conv) were statistically significant ($P < .001$) for all metrics except HI. The Δ% values of D_{max} and D_{98} for sConv versus Conv were smaller than TMR10 versus Conv by approximately 6% and 11%, respectively, for cross-validation and internal validation sets.

Comparison between the γ pass rates with the 1 mm/1% criterion of TMR10 dose (74.18 ± 15.77%) and sConv dose (92.43 ± 8.60%) to the Conv dose as a reference dose showed a significant difference in the cross-validation set ($P \leq .001$). The internal validation set also

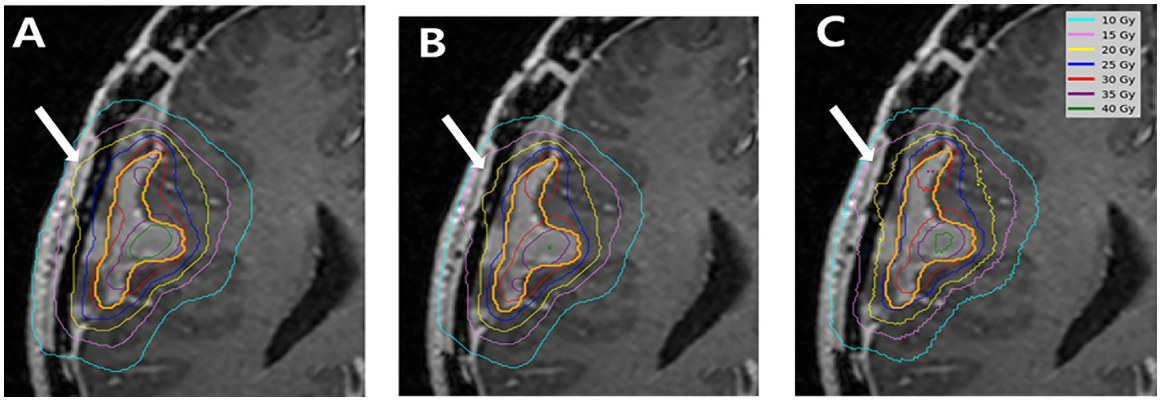

Figure 2 TUMOR contour (orange) and isodose lines of (A) TMR10 dose, (B) Conv dose, and (C) sConv dose in the second column of Figure 1B for 10 to 40 Gy with prescription dose of 25 Gy. The white arrow points to the 20 Gy isodose line (yellow), where the heterogeneity correction was significant because of a skull structure. sConv dose shows isodose lines comparable to the Conv dose compared to the TMR10 dose to the Conv dose.
Abbreviations: Conv = convolution; sConv = synthetic convolution.

Table 2 Quantitative comparison of TMR10, Conv, and sConv dose

	Cross-validation set			Internal validation set		
Parameter	Δ% (TMR10, Conv)	Δ% (sConv, Conv)	*P* value	Δ% (TMR10, Conv)	Δ% (sConv, Conv)	*P* value
D_{max}	8.14 ± 1.60	3.59 ± 3.59	<.001*	8.28 ± 1.09	1.22 ± 0.77	<.001*
D_2	8.04 ± 1.60	2.87 ± 2.15	<.001*	7.69 ± 2.65	2.62 ± 2.73	<.001*
D_{50}	8.35 ± 1.69	2.37 ± 2.13	<.001*	8.74 ± 1.62	1.40 ± 1.19	<.001*
D_{mean}	8.64 ± 1.92	2.21 ± 1.85	<.001*	8.97 ± 1.52	1.37 ± 1.11	<.001*
D_{98}	13.62 ± 8.11	4.89 ± 5.97	<.001*	14.00 ± 7.17	3.56 ± 4.07	<.001*
D_{min}	19.64 ± 17.59	11.04 ± 15.90	<.001*	18.28 ± 9.86	6.51 ± 4.40	<.001*
HI	5.87 ± 5.76	8.07 ± 6.90	.007	13.15 ± 10.40	11.87 ± 8.64	.37

Abbreviations: Conv = convolution; sConv = synthetic convolution; D_2 = dose that 2 % or less of the tumor volume received; D_{50} = dose that 50% of the tumor volume received; D_{98} = dose that 98% of the tumor volume received; D_{max} = maximum tumor dose; D_{mean} = mean tumor dose; D_{min} = minimum tumor dose; HI = homogeneity index.
*Statistically significant values. $P < .007$ is significant after Bonferroni correction.

demonstrated a substantial difference between the γ pass rates (TMR10 dose, 65.84 ± 14.29 %; sConv dose, 96.40 ± 3.99 %).

Table E1 presents the isodose dice between the TMR10 and Conv doses and between the sConv and Conv doses at various isodose levels. Statistically significant improvement of isodose volume similarity was found for all metrics for 10%, 30%, 50%, 70%, and 90% isodose levels, where 50% was the prescription isodose level. Significantly, the sConv dose showed much higher isodose volume similarities to the Conv dose for the isodose volume of lower isodose (10%-50%) than the isodose levels higher than the prescription dose level (ie, 70% and 90% isodose volume dice). Isodose volume similarity at all isodose levels is plotted in Fig. E3.

Dose distribution dependence on skull-to-tumor distance

Table 3 shows the γ pass rates and prescription isodose dice for tumors near the skull. The γ pass rates of TMR10 dose relative to Conv dose were lower for tumors near the skull (cross-validation, 67.38 ± 14.36 % [n = 27]; internal validation, 60.26 ± 11.48 % [n = 4]) than the tumors not near to the skull (cross-validation 76.70 ± 15.41 % [n = 73]; internal validation, 67.08 ±14.16 % [n = 18]). The prescription isodose dice between TMR10 and Conv doses were also lower for tumors near the skull than those not near the skull. Meanwhile, sConv doses demonstrated much more improved γ pass rates for tumors in all locations: in cross-validation (<2 cm, 92.50 ± 7.05 %; ≥2 cm,

Table 3 Skull-to-tumor distance-dependent model performance on predicting the heterogeneity effect

Cross-validation set						
	Skull-to-tumor distance					
	<2 cm (n = 27)			≥2 cm (n = 73)		
Parameters	TMR10 dose	sConv dose	*P* value	TMR10 dose	sConv dose	*P* value
Gamma index pass rate (%)	67.38 ± 14.36	92.50 ± 7.05	<.001*	76.70 ± 15.41	92.41 ± 9.06	<.001*
Prescription isodose dice (%)	88.97 ± 3.10	91.19 ± 4.11	.001*	90.06 ± 4.00	91.97 ± 5.24	<.001*
Internal validation set						
	Skull-to-tumor distance					
	<2 cm (n = 4)			≥2 cm (n = 18)		
Parameters	TMR10 dose	sConv dose	*P* value	TMR10 dose	sConv dose	*P* value
Gamma index pass rate (%)	60.26 ± 11.48	98.58 ± 1.10	.12	67.08 ± 14.16	95.92 ± 4.13	<.001*
Prescription isodose dice (%)	91.22 ± 0.92	97.25 ± 0.87	.12	90.25 ± 2.31	94.27 ± 1.86	.001*

Abbreviation: sConv = synthetic convolution.
*Statistically significant values.

Table 4 Tumor volume dependent model performance on predicting the heterogeneity effect

Cross-validation set						
	Tumor volume					
	<1 cm^3 (n = 8)			≥1 cm^3 (n = 92)		
Parameters	TMR10 dose	sConv dose	*P* value	TMR10 dose	sConv dose	*P* value
Gamma index pass rate (%)	87.66 ± 18.56	87.45 ± 15.44	.54	74.07 ± 15.73	92.42 ± 8.60	<.001*
Prescription isodose dice (%)	83.56 ± 7.11	82.79 ± 7.48	.54	90.31 ± 2.78	92.54 ± 3.80	<.001*
Internal validation set						
	Tumor volume					
	<1 cm^3 (n = 1)			≥1 cm^3 (n = 21)		
Parameters	TMR10 dose	sConv dose	*P* value	TMR10 dose	sConv dose	*P* value
Gamma index pass rate (%)	74.46	93.48	1	65.43 ± 14.16	96.54 ± 3.94	<.001*
Prescription isodose dice (%)	91.42	91.32	1	90.38 ± 2.20	94.98 ± 1.97	<.001*

Abbreviation: sConv = synthetic convolution.
*Statistically significant values.

92.41 ± 9.06 %) and internal validation sets (<2 cm, 98.58 ± 1.10 %; ≥2 cm, 95.92 ± 4.13 %). Prescription isodose dice are also improved in sConv dose for cross-validation and internal validation sets.

Dose distribution dependence on the tumor size

The dependence of the model performance on the tumor size is evaluated in Table 4. The heterogeneity effect is well predicted for tumors larger than 1 cm^3 for cross-validation and internal validation sets. The γ pass rates of 94.42 ± 8.60 % and 96.54 ± 3.94 % were achieved for the sConv dose in the cross-validation set (n=92) and internal validation set (n = 21), respectively, whereas the TMR10 dose had 74.07 ± 15.73 % and 65.43 ± 14.16 %. For tumors < 1 cm^3, the sConv dose and TMR10 dose showed a similar average γ pass rate of approximately 87% in the cross-validation set (n = 8). On the contrary, the sConv dose in the internal validation set (n = 1) showed a γ pass rate of 93.48 %, whereas the TMR10 dose showed a γ pass rate of 74.46%. However, the difference between sConv versus Conv and TMR10 versus Conv cannot be confirmed with only 1 patient. The prescription isodose dice from the cross-validation and internal validation sets also showed a similar tendency of comparable γ pass rate and isodose dice for tumors with size < 1 cm^3, and those were even higher for tumors with size > 1 cm^3.

Discussion

LINAC-based planning systems incorporate tissue inhomogeneity corrections within their dose calculations, whereas GKRS commonly uses the TMR-10 homogeneous water-density-based calculations in routine clinical settings.[22] Recent studies have shown noticeable differences (4%-9%) between the doses calculated by the TMR10 and the convolution methods.[23-27] It is noted that the 4% to 9% dose difference can significantly impact tumor coverage and the occurrence of radiation damage to sensitive critical structures near the tumor, including the healthy brain. Typical prescription doses for single-fraction stereotactic radiosurgery treatments of solitary metastases range from 15 to 24 Gy. The constraint of V_{12} (the volume of healthy brain tissue receiving 12 Gy or more) ≤ 5 to 10 cc is used to minimize the risk of radiation necrosis.[28] In these cases, a 9% calculated dose difference may influence whether a clinician accepts or rejects a GKRS plan or chooses to fractionate the treatment. Furthermore, clinicians often evaluate GKRS plans by considering dose constraints to the optic and auditory structures, such as the lens, orbit, optic nerves, and cochlea, which exhibit toxicity to low doses of radiation.[29] Slight differences in calculated radiation dose can impact hearing and vision outcomes.

Deep learning-based treatment planning demonstrated a potential for automatic treatment planning while it still suffered from predicting the accurate dose distribution to healthy tissues.[7-12] To overcome the current limitations, we developed a cGAN-based sConv dose calculation system as an efficient and accurate method to bridge the gap between convolution-based inhomogeneity-corrected and TMR10-based GKRS planning. The conditional GAN generated sConv doses qualitatively and quantitatively similar to Conv doses in the cross-validation and internal validation sets. The relationship between the isodose lines and the tumor volume of Conv dose was well preserved in sConv. The trained model could accurately predict the dose distributions accounting for the effects of increased

attenuation and scattering by the bony skull. Furthermore, the validity of the new algorithm was demonstrated by the data indicating the skull-to-tumor distance dependence of the dose distributions. Differences between the TMR10 and Conv doses were more significant for tumors near the skull, whereas the sConv dose showed significantly improved similarity with the Conv dose. The tissue heterogeneity effect was well predicted for tumors with size > 1 cm^3 by the model.

Our qualitative and quantitative analyses showed the effectiveness of the sConv dose for understanding the change in dose delivery because of skull-induced scatter and attenuation. sConv dose could be used to find potentially uncovered tumor areas with a dose significantly lower than the prescription dose. Moreover, in stereotactic radiosurgery, setting a 50% isodose line as a prescription dose to a tumor volume and having a hot spot in the center of the tumor helps the tumor control probability without a chance of adding toxicity. Thus, correctly knowing that there will not be hot spots in the center of the tumor volume may enforce replanning for optimally including hot spots in the tumor volume.

We must acknowledge some limitations in our study. First, registration errors prevented the model from accurately learning the dose distribution. Thus, about 30% of patients' data were not used in this study because we observed that the coregistration between MR and CT images was erroneous after visual examination. Since the calculated doses of TMR10 and Conv were attached to MR and CT data independently, the imprecise coregistration could result in a misleading comparison between TMR10 and Conv. However, our data selection procedure and the criteria were not determined using a solid mathematical theory or evidence. Thus, the impact of the coregistration errors must be thoroughly studied in the future. Second, the heterogeneity prediction on the small tumors (<1cm^3) did not demonstrate improved similarity to the Conv dose. The calculation time of the Conv dose for small tumors is short enough not to disturb the clinical workflow. Thus, in practice, the convolution algorithm with CT can be applied to examine the heterogeneity effects for small tumors, and our model could be implemented only for non-small tumor cases. Third, our study's participants mainly consisted of patients with metastatic tumors; hence, including diverse brain cancer cohorts can improve the model's generalizability. Lastly, our data lack patients with multiple tumors. Developing the advanced deep learning model to capture global features from the 3-dimensional dose distribution may be effective for further investigating patients with multiple tumors.

Conclusions

Our deep learning-generated heterogeneity-corrected dose distribution demonstrated strong correlations with actual convolution doses for single brain cancers in GKRS. Using an advanced generative model and collecting more patient data will further improve the study's validity and the implications of the model in clinical settings in the future.

Disclosures

The authors declare that they have no known competing financial interests or personal relationships that could have appeared to influence the work reported in this paper.

Acknowledgments

The Minnesota Supercomputer Center (MSI) at the University of Minnesota provided the computing resources required to perform the model training for this study. URL: http://www.msi.umn.edu. This manuscript is based on work previously presented at the 66th Annual Meeting of the American Association of Physicists in Medicine (AAPM), held in Los Angeles, California in 2024, as a poster titled "Prediction of Heterogeneous Treatment Planning in Gamma Knife Radiosurgery Using Homogeneous Plan with Conditional Generative Adversarial Network".

Supplementary materials

Supplementary material associated with this article can be found in the online version at doi:10.1016/j.adro.2025.101757.

References

1. Rojas-Villabona A, Kitchen N, Paddick I. Investigation of dosimetric differences between the TMR 10 and convolution algorithm for Gamma Knife stereotactic radiosurgery. *J Appl Clin Med Phys*. 2016;17:217-229.
2. Duggar WN, He R, Bhandari R, et al. Considering inhomogeneities in Gamma Knife treatment planning: Factors affecting the loss of prescription dose coverage. *J Radiosurg SBRT*. 2020;6:303-310.
3. Chen WZ, Xiao Y, Li J. Impact of dose calculation algorithm on radiation therapy. *World J Radiol*. 2014;6:874-880.
4. Watanabe Y, Mathew D, Natanasabapathi G. A practical strategy for incorporating the convolution algorithm in Leksell GammaPlan for routine treatment planning. *J Radiosurg SBRT*. 2022;8:297-303.
5. Kaji S, Kida S. Overview of image-to-image translation by use of deep neural networks: denoising, super-resolution, modality conversion, and reconstruction in medical imaging. *Radiol Phys Technol*. 2019;12:235-248.
6. Ho J, Jain A, Abbeel P. Denoising diffusion probabilistic models. In: Larochelle H, Ranzano M, Hadsell R, Balcan MF, Lin H, eds. *Proceedings of the 34th International Conference on Neural Information Processing Systems*. Curran Associates Inc; 2020:6840-6851.
7. Zhang Y, Li C, Zhong L, Chen Z, Yang W, Wang X. DoseDiff: distance-aware diffusion model for dose prediction in radiotherapy. *IEEE Trans Med Imaging*. 2024;43:3621-3633.

8. Feng Z, Wen L, Wang P, et al. DiffDP: radiotherapy dose prediction via a diffusion model. In: Greenspan H, Madabhushi A, Mousavi P, eds. Medical Image Computing and Computer Assisted Intervention – MICCAI2023: 26th International Conference, Vancouver, BC, Canada, October 8–12, 2023, Proceedings, Part VI. Springer-Verlag; 2023:191-201.
9. Zhang B, Babier A, Chan TCY, Ruschin M. 3D dose prediction for Gamma Knife radiosurgery using deep learning and data modification. *Phys Med*. 2023;106:102533.
10. Kearney V, Chan JW, Wang T, et al. DoseGAN: a generative adversarial network for synthetic dose prediction using attention-gated discrimination and generation. *Sci Rep*. 2020;10:11073.
11. Gao R., Lou B., Xu Z., Comaniciu D., Kamen A. Flexible-Cm GAN: towards precise 3D dose prediction in radiotherapy. In: Gao R., Lou B., Xu Z., Comaniciu D., Kamen A., eds, Proceedings of the IEEE/CVF Conference on Computer Vision and Pattern Recognition (CVPR). IEEE; 2023: 715-725.
12. Zhan B, Xiao J, Cao C, et al. Multi-constraint generative adversarial network for dose prediction in radiotherapy. *Med Image Anal*. 2022;77:102339.
13. Lee S, Watanabe Y. Prediction of heterogeneous treatment planning in Gamma Knife radiosurgery using homogeneous plan with conditional generative adversarial network. *66th Annual Meeting & Exhibition AAPM 2024*. Los Angeles, CA; July 21, 2024.
14. Chen Y, Yang XH, Wei Z, et al. Generative adversarial networks in medical image augmentation: a review. *Comput Biol Med*. 2022;144:105382.
15. Goodfellow I, Pouget-Abadie J, Mirza M, et al. Generative adversarial nets. In: Ghahramani Z, Welling M, Cortes C, Lawrence N, K.Q. Weinberger KQ, eds. *Advances in Neural Information Processing Systems*. Curran Associates, Inc.; 2014:2672-2680.
16. Palmér E, Karlsson A, Nordström F, et al. Synthetic computed tomography data allows for accurate absorbed dose calculations in a magnetic resonance imaging only workflow for head and neck radiotherapy. *Phys Imaging Radiat Oncol*. 2021;17:36-42.
17. Wyatt JJ, Kaushik S, Cozzini C, et al. Comprehensive dose evaluation of a Deep Learning based synthetic Computed Tomography algorithm for pelvic Magnetic Resonance-only radiotherapy. *Radiother Oncol*. 2023;184:109692.
18. Isola P, Zhu J-Y, Zhou T, Efros AA. Image-to-image translation with conditional adversarial networks. *2017 IEEE Conference on Computer Vision and Pattern Recognition (CVPR)*. IEEE Computer Society; 2017:5967-5976.
19. Chaikh A, Desgranges C, Balosso J. The use of gamma indices with medical imaging as quality assurance tool to validate the dose calculation algorithm in the modern practice of medical physics. *Nucl Med Biomed Imaging*. 2016;1.
20. Bodensohn R, Maier SH, Belka C, Minniti G, Niyazi M. Stereotactic radiosurgery of multiple brain metastases: a review of treatment techniques. *Cancers (Basel)*. 2023;15:5404.
21. Mould RF. *Introductory Medical Statistics*. 3rd ed. Institute of Physics Publishing; 1995.
22. Peters GW, Tien CJ, Chiang V, Yu J, Hansen JE, Aneja S. Impact of tissue heterogeneity correction on Gamma Knife stereotactic radiosurgery of acoustic neuromas. *J Radiosurg SBRT*. 2021;7:207-212.
23. Fallows P, Wright G, Harrold N, Bownes P. A comparison of the convolution and TMR10 treatment planning algorithms for Gamma Knife® radiosurgery. *J Radiosurg SBRT*. 2018;5:157-167.
24. Moskvin V, Timmerman R, DesRosiers C, et al. Monte Carlo simulation of the Leksell Gamma Knife: II. Effects of heterogeneous versus homogeneous media for stereotactic radiosurgery. *Phys Med Biol*. 2004;49:4879-4895.
25. Nakazawa H, Komori M, Shibamoto Y, Tsugawa T, Mori Y, Kobayashi T. Dosimetric comparison of absolute and relative dose distributions between tissue maximum ratio and convolution algorithms for acoustic neuroma plans in Gamma Knife radiosurgery. *Acta Neurochir*. 2014;156:1483-1489.
26. Xu AY, Bhatnagar J, Bednarz G, et al. Dose differences between the three dose calculation algorithms in Leksell GammaPlan. *J Appl Clin Med Phys*. 2014;15:4844.
27. Xu AY, Bhatnagar J, Bednarz G, et al. Gamma Knife radiosurgery with CT image-based dose calculation. *J Appl Clin Med Phys*. 2015;16:119-129.
28. Milano MT, Grimm J, Niemierko A, et al. Single- and multifraction stereotactic radiosurgery dose/volume tolerances of the brain. *Int J Radiat Oncol Biol Phys*. 2021;110:68-86.
29. Hanna GG, Murray L, Patel R, et al. UK consensus on normal tissue dose constraints for stereotactic radiotherapy. *Clin Oncol (R Coll Radiol)*. 2018;30:5-14.